

# NAVIS: A LAMMPS-Python framework for efficient computation of nanochannel velocity and thermal interfacial slip

Sleeba Varghese<sup>a,\*</sup>, Sabin Alosious<sup>b</sup>, J. S. Hansen<sup>c</sup>, B. D. Todd<sup>d</sup>

<sup>a</sup>*Sorbonne Université, CNRS, Laboratoire PHENIX (Physicochimie des Electrolytes et Nanosystèmes Interfaciaux), 4 place Jussieu, 75005 Paris, France*

<sup>b</sup>*Aerospace and Mechanical Engineering Department, The University of Notre Dame, Notre Dame, IN 46556, USA*

<sup>c</sup>*“Glass and Time”, IMFUFA, Department of Science and Environment, Roskilde University, Roskilde 4000, Denmark*

<sup>d</sup>*Department of Mathematics, School of Science, Computing and Emerging Technologies, Swinburne University of Technology, John Street, Hawthorn, Victoria 3122, Australia*

## Abstract

We present NAVIS (NAnochannel Velocity and thermal Interfacial Slip), a LAMMPS-Python scripted toolkit for computing the Navier (hydrodynamic) friction coefficient and Kapitza (thermal) resistance at arbitrary solid-fluid interfaces. NAVIS is based on equilibrium molecular dynamics (EMD) methods for calculating the linear response friction and thermal resistance at the interface, as well as the corresponding velocity and temperature slips. The methodology is based on our previous studies (Hansen, *et al.*, Phys. Rev. E **84**, 016313 (2011); Varghese *et al.*, J. Chem. Phys. **154**, 184707 (2021); Alosious, *et al.*, J. Chem. Phys. **151**, 194502 (2019); Alosious, *et al.*, Langmuir **37**, 2355-2361 (2021)), and in this work we provide a pedagogical framework for the implementation of this toolkit on two systems: (i) a water-graphene system (for hydrodynamic slip) and (ii) a water-CNT system (for thermal slip). We provide detailed instructions for performing the EMD simulations using the LAMMPS package and processing the simulation outputs using Python modules to obtain the desired quantities of interest. We expect the toolkit to be useful for computational researchers studying interfacial friction and thermal transport, key factors for efficient and practical applications of nanofluidic systems.

**Keywords:** Navier friction coefficient; Kapitza resistance; velocity slip; thermal slip; molecular dynamics.

## PROGRAM SUMMARY

*Program Title:* NAVIS

*CPC Library link to program files:* (to be added by Technical Editor)

*Developer's repository link:* <https://github.com/sleebaslv/NAVIS>

*Licensing provisions:* GNU General Public License v3.0

*Programming language:* Python 3

*Nature of problem:* Measure the interface-intrinsic hydrodynamic and thermal resistance at the solid-fluid boundary using equilibrium molecular dynamics (EMD) simulations.

*Solution method:* Creating a Python-based code to compute hydrodynamic and thermal interfacial friction coefficients from data obtained via EMD simulations conducted using LAMMPS.

## 1. Introduction

The study of friction and heat transfer at the solid-liquid interface has in recent years become a focus of intensified research. At its heart lays the prospect of improving lubrication technologies to minimise energy losses due to friction (tribology) whilst also improving heat exchange efficiency - either to ensure maximum heat exchange for cooling purposes or the opposite if insulation is required. Driving this study is climate

change and the urgency to reduce greenhouse gas emissions, whilst simultaneously improving energy efficiency in mechanical devices and batteries. It is not widely known that 23% of global energy consumption is due to tribological contacts and that 20% of this is due to the energy required to overcome friction, including the friction generated in electric vehicles [1]. Clearly then, increased knowledge of friction and thermal energy transfer at the crucial solid-liquid interface is highly sought after and many studies involving experiment, theory and computer simulation are devoted to this [2, 3, 4, 5, 6, 7].

From a conceptual perspective, the friction that exists between the solid wall and fluid can be understood as the ability/inability of the interfacial fluid to experience “slip” along the solid surface. Slip is defined as the departure of a corresponding observable (velocity for hydrodynamic slip and temperature for thermal slip) from the no-slip boundary condition, and its effect becomes significant when the confinement width reduces to nanometric scales. The hydrodynamic and thermal slips are often characterized in terms of interfacial transport coefficients, namely Navier friction coefficient (for hydrodynamic friction) and Kapitza resistance (for thermal friction), respectively. Hence, efficient design of nanoscale systems requires theoretical/computational frameworks that can provide precise estimates of these transport coefficients, consistent with the nature of the solid-fluid interface under consideration.

Various computational approaches are available to calculate

\*Corresponding author.

E-mail address: sleeba.varghese@sorbonne-universite.fr

interfacial transport properties such as friction and thermal resistance. Broadly, these methods can be classified into equilibrium molecular dynamics (EMD) approaches, which exploit linear-response theory and yield properties that are directly comparable to experimental observables, and nonequilibrium molecular dynamics (NEMD) approaches, which impose external driving fields to probe the system's response. While NEMD techniques can access nonlinear regimes, it is unfeasible to generate statistically reliable flow fields at experimentally relevant external field strengths and consequently extrapolation techniques must be employed to obtain friction coefficient values at experimentally achievable field strengths [8]. This drawback of NEMD techniques becomes particularly noticeable for high-slip systems, as demonstrated by Kannam *et al.* [9, 10], making linear-response theory based techniques (EMD) the preferred choice. However recent developments, such as the transient-time correlation function (TTCF) method [11, 12, 13, 14], now enable direct NEMD simulations at physically meaningful rates of strain and can be implemented in conjunction with the LAMMPS package [14]. Given the generality and accuracy of the linear-response theory under normal laboratory conditions, in this work we primarily focus on the computation of friction and thermal resistance using EMD simulations.

To our knowledge, the first linear response model to predict the friction coefficient at the solid-fluid interface was that of Bocquet and Barrat [15]. Their method involves a Green-Kubo-like integration of a time-autocorrelation function of tangential interfacial forces, performed at equilibrium. Bocquet and Barrat do warn users that such a formulation for confined systems must be treated with caution, noting that: "... the evaluation of these formulas leads in finite systems to vanishing transport coefficients" and "To obtain a nonvanishing transport coefficient... the thermodynamic limit must be taken." In short, if one does not truncate the correlation function at some point in delay-time, it diverges and the corresponding integral vanishes, leading to an under-estimate for the friction coefficient and hence slip lengths that are higher than they should be. The source of this divergence is the fact that Green-Kubo methods are intrinsically applicable to systems that are at zero-wavevector, i.e. unconfined "bulk" systems, or as Bocquet and Barrat state are in "the thermodynamic limit". This divergence is clearly demonstrated in reference [16] and discussions can be found in references [8, 17, 18, 19]. For MD simulations this becomes a computational bottleneck. Several authors have proposed practical strategies to address this issue [20, 21, 22, 23, 24, 25, 26, 27], and the reader is referred to these works for more information on this methodology. The theoretical foundations of this non-zero wavevector divergence can be found in the books by Hansen and McDonald [28], Evans and Morriss [18] and Todd and Daivis [8]. Petracic and Harrowell [19, 29] also pointed out that by integrating over the entire volume of the confined fluid, the friction coefficient determined includes the viscous resistance of the fluid itself, and so is not an intrinsic friction coefficient.

In an attempt to remove altogether the controversy of applying Green-Kubo-like methods to confined (non-zero wavevector) systems, Hansen *et al.* [30] proposed an alternative lin-

ear response (equilibrium MD) method that did not involve an integration over the volume of the fluid. It has the additional advantage of being able to calculate the solid-fluid friction coefficients for a fluid confined by two different solid walls during a single simulation, i.e. obtaining two unique intrinsic friction coefficients reflective of the two different confining surfaces. In contrast, the Bocquet-Barrat method can only obtain an effective friction coefficient for such a system, in which it is a hybrid of both interfaces. Recently, Varghese *et al.* [16] proposed an improvement to the method of Hansen *et al.* that increased its statistical accuracy, and it is this latter implementation we reproduce and implement in this work.

In an entirely analogous fashion, the calculation of the weak-field (linear response) Kapitza resistance can be formulated by either a Green-Kubo-like correlation function integral proposed by Barrat and Chiaruttini [31] or by the non-integral time-correlation approach proposed by Alosious *et al.* [32, 33]. As with the case of the friction coefficient, the former method involves an integral which *diverges* at long times, whereas the latter does not, as clearly shown in reference [33]. In this work, we implement the calculation proposed by Alosious *et al.* [33] because of its stability and statistical accuracy.

The motive of the present work is to provide a useful computational toolkit, implemented in Python [34] and interfaced with the popular LAMMPS software package [35], that can readily compute the Navier friction coefficient and Kapitza resistance for arbitrary solid-fluid interfaces. The following section briefly discusses the theoretical framework behind the hydrodynamic and thermal friction computing methodologies. The subsequent sections provide detailed descriptions of the simulation and post-processing procedures used to compute the Navier friction coefficient and Kapitza resistance, followed by a results and discussion section, where we present some important results obtained using the proposed methodologies.

## 2. Theory

In this section we briefly outline the mathematical formulation to compute the required quantities. Full details of the theory and validation are found in the original papers on slip [30, 16] and Kapitza resistance [32, 36, 33, 37], and the reader is encouraged to refer to them for more details.

The basic idea proposed for the calculation of the Navier friction coefficient and the Kapitza resistance is that they are both *local* interfacial properties that are dominated by interactions between molecules in the immediate fluid layer adjacent to the fluid and the corresponding wall atoms. Time-correlation functions are formed between relevant quantities based upon the defining constitutive equation, equilibrium molecular dynamics simulations on the system of interest are performed, and then the Navier friction coefficient or Kapitza resistance is extracted from the relevant time-correlation data. The fundamental expressions are summarised below.

### 2.1. Navier Friction coefficient

Let a fluid system be confined between solid walls separated some distance  $L_z$  in the  $z$ -direction, as shown in Figure 1. We

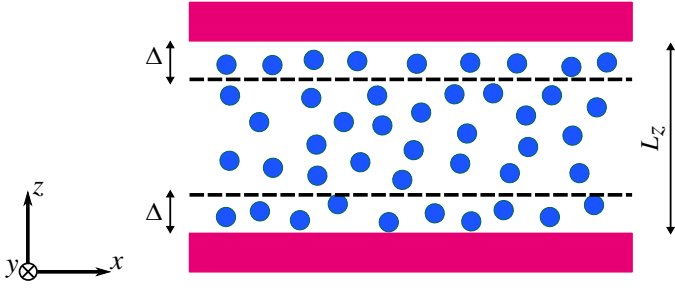


Figure 1: A 2-D schematic diagram of the fluid molecules (depicted as solid circles) confined by planar walls. The actual system is three-dimensional and periodic in the  $x$  and  $y$  directions.  $\Delta$  is the slab width.

assume that the zero-frequency friction coefficient ( $\xi_0$ ) is defined in the usual manner, namely  $\sigma_{xy} = \xi_0 u_s$ , where  $\sigma_{xy}$  and  $u_s$  are, respectively, the shear stress and slip velocity measured at the solid-fluid interface. If we assume that any (linear response) flow is in the  $x$ -direction and the system is periodic in both the  $x$  and  $y$  directions, then we can define  $u_x(t)$  to be the  $x$ -component velocity of a slab of fluid of width  $\Delta$  in the  $z$ -direction immediately adjacent to the wall and  $F_x(t)$  to be the  $x$ -component of force between all fluid atoms in the slab and all wall atoms. If we define the time-correlation functions

$$C_{u_x F_x}(t) \equiv \langle u_x(0) F_x(t) \rangle \text{ and } C_{u_x u_x}(t) \equiv \langle u_x(0) u_x(t) \rangle \quad (1)$$

and we denote the Laplace transform of an arbitrary function of time  $f(t)$  as

$$L[f(t)] = \int_0^\infty f(t) e^{-st} dt \equiv \tilde{f}(s), \quad (2)$$

then  $\xi_0$  is obtained as

$$\xi_0 = \frac{B_1}{A \lambda_1} \quad (3)$$

where  $B_1$  and  $\lambda_1$  are parameters of a one-term Maxwellian memory function descriptive of the friction coefficient, defined as

$$\zeta(t) = B_1 e^{-\lambda_1 t} \quad (4)$$

and  $A$  is the surface area of the solid-liquid interface.  $B_1$  and  $\lambda_1$  are obtained by Laplace transforming the time-correlation functions obtained from molecular dynamics simulations, as described by Hansen *et al.* in their original paper [30]. This leads to the following expression in Laplace-space:

$$\tilde{C}_{u_x F_x}(s) = -\frac{B_1}{s + \lambda_1} \tilde{C}_{u_x u_x}(s). \quad (5)$$

Performing a regression fit to Eq (5) leads to robust and reliable values of the friction coefficient, from which the slip velocity and slip length may also be accurately predicted. While this is sufficient, Varghese *et al.* [16] later demonstrated that even higher statistical accuracy could be obtained by numerically integrating along the Laplacian domain to compute  $B_1$  and  $\lambda_1$ . By integrating Eq (5) between arbitrary points  $s_1$  and  $s_2$  and also  $s_3$  and  $s_4$  in Laplace-space the following two sets of equations

are obtained:

$$\frac{1}{B_1} \left[ \frac{s_2^2 - s_1^2}{2} + \lambda_1 (s_2 - s_1) \right] = \Lambda_1 \quad (6)$$

$$\frac{1}{B_1} \left[ \frac{s_4^2 - s_3^2}{2} + \lambda_1 (s_4 - s_3) \right] = \Lambda_2 \quad (7)$$

where  $\Lambda_i \equiv - \int_{s_i}^{s_j} \frac{\tilde{C}_{u_x u_x}(s)}{\tilde{C}_{u_x F_x}(s)} ds$  and  $j > i$ . Defining  $C \equiv \Lambda_1/\Lambda_2$  and dividing Eq (6) by Eq (7) gives the expression for  $\lambda_1$  as

$$\lambda_1 = \frac{\left( s_2^2 - s_1^2 - C(s_4^2 - s_3^2) \right)}{2(C(s_4 - s_3) - s_2 + s_1)}. \quad (8)$$

$B_1$  is then easily obtained by substituting  $\lambda_1$  into either Eq (6) or Eq (7). It is this latter technique that we use to obtain the friction coefficient  $\xi_0$  via Eq. (3).

## 2.2. Kaptiza resistance

Let us assume the same system geometry as above, only there is no assumed momentum flow and the only flow of interest is that of heat. The Kaptiza resistance,  $R_k$ , is defined as  $R_k \equiv \Delta T/J_q = 1/G_k$ , where  $\Delta T$  is the difference between the temperature of the solid interface and a molecularly thin liquid layer immediately adjacent to it,  $J_q$  is the interfacial heat flux normal to the surface and  $G_k$  is the interfacial thermal conductance. In an analogous manner to the friction coefficient derivation, we find that [33]

$$\tilde{C}_{T J_q}(s) = \tilde{G}_k(s) \tilde{C}_{TT}(s) \quad (9)$$

where  $C_{T J_q}(t) \equiv \langle T(0) J_q(t) \rangle$  and  $C_{TT}(t) \equiv \langle T(0) T(t) \rangle$ . Note here that although we follow the specific form of the derivation presented in reference [33], an alternative derivation making use of the interfacial heat flux autocorrelation function was the original version of this methodology [32]. It was later found that using the temperature autocorrelation function yielded statistically superior values of Kaptiza resistance and temperature slip predictions, so we only present that version even though both implementations can be used to predict  $R_k$  and temperature slip. Expressing the instantaneous  $G_k$  as a one-term Maxwellian,  $G_k(t) = k_1 e^{-\mu_1 t}$ , we find from Eq (9)

$$\tilde{C}_{T J_q}(s) = \frac{k_1}{s + \mu_1} \tilde{C}_{TT}(s). \quad (10)$$

$k_1$  and  $\mu_1$  are obtained by regression fits to the equilibrium molecular dynamics time-correlation function data, giving us

$$R_k = \frac{1}{G_k} = \frac{\mu_1}{k_1}. \quad (11)$$

The reader is referred to Ref 32 for further details, including how to compute  $J_q$  at the interface, and to Ref 33 to know more about the implementation of this methodology to cylindrical wall geometries. It is interesting that the Kaptiza resistance computed by this method is statistically superior to the friction coefficient computed by the analogous method first proposed by Hansen *et al.* [30]. For this reason, we have found no need to extend this method to a form similar to that of Varghese *et al.*'s

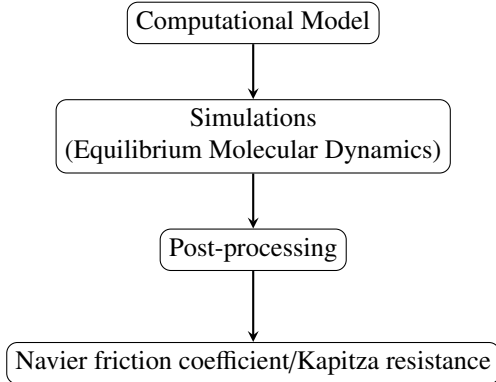


Figure 2: Flowchart outlining the steps involved in the computation of the Navier friction coefficient or Kapitza resistance.

[16] method to enhance the statistical accuracy of the friction coefficient calculation. Computation of the so-called temperature slip will also be demonstrated later. Unless explicitly stated otherwise, from hereon the term “slip” is to be understood as denoting either hydrodynamic (velocity) or thermal (temperature) slip.

### 3. Computational Methodology

In this section, we explain the simulation and post-processing methodologies used to compute the interfacial slip in a nanoconfined system. Fig 2 shows the essential steps involved in our NAVIS framework, and in the subsequent subsections we explain each of these steps in detail. The codes and scripts corresponding to the following sections are publicly accessible via GitHub, and the repository structure is described in Appendix B.

#### 3.1. Model

The effect of interfacial slip becomes a contributing factor to the fluid flow or heat-exchange rate only when the confinement width reduces to nanometric scales [10, 3]. In our previous works, we used the NAVIS methodology to compute the interfacial slip for different fluids confined in planar nanochannels [38, 16, 39, 36] and cylindrical nanopores [40, 10, 33]. The results presented in this work are taken from either of these previous studies, and the reader is referred to the above mentioned articles for additional details on the system setup for the specific geometry of choice. Once the computational model has been built, the next step is to perform equilibrium simulations of the model to measure the fluctuations of the relevant properties.

#### 3.2. Simulations

For equilibrium simulations, we use molecular dynamics (MD) as our simulation protocol. MD simulations involve numerically solving the Newtonian equations of motion for each particle in the system using appropriate numerical schemes [41, 42] and for the purpose of our studies we used

the Large-scale Atomic/Molecular Massively Parallel Simulator [43] (LAMMPS) package for performing the simulations. The systems are maintained at thermal equilibrium using the thermostating schemes available in LAMMPS. In our simulations, thermal equilibration is achieved by thermostating the confining walls rather than the fluid itself, a strategy that has been shown to be the appropriate methodology when working with nanoconfined systems [44, 45, 46]. Algorithm 1 shows the relevant steps involved in an EMD simulation in LAMMPS to extract the relevant quantities for computing hydrodynamic or thermal slip.

---

**Algorithm 1** LAMMPS simulation procedure for interfacial slip

---

```

1: Initialize the system.
2: Run  $N_{eq}$  timesteps for equilibration.
3: Define the slab region.
4: Define the slab as a dynamic group with the atoms being
   updated at every timestep.
5: if slip = hydrodynamic slip then
6:   for each step  $t$  from 1 to  $N$  do
7:     Compute the force acting on the slab due to the
   wall.
8:     Compute the center of mass velocity of the slab.
9:     Save the force component and the center of mass
   velocity.
10:  end for
11: end if
12: if slip = thermal slip then
13:   for each step  $t$  from 1 to  $N$  do
14:     Compute the temperature difference between the
   solid and fluid slab.
15:     Compute the heat flux between the solid and fluid
   slab.
16:     Save the heat flux and temperature difference.
17:  end for
18: end if
  
```

---

As mentioned in Sec 2, one of the hallmarks of our slip methodology is that we restrict our zone of interest to a few molecular diameters away from the wall. This avoids the possible interference of the bulk fluid contributions and hence makes the slip estimated using this methodology an intrinsic parameter of the solid-liquid interface. To be consistent with the theoretical framework proposed by Hansen *et al.* [30], the simulations must ensure that the relevant quantities are only averaged over the interfacial region of particles. This objective is achieved using the *dynamic group* feature available in LAMMPS. The code snippet shown in Listing 1 provides the syntax for implementing this feature to compute the Navier friction coefficient. Similarly, Listing 2 shows the code snippet for the Kapitza resistance. We also mention here that we use the terminology “slab” to define the interfacial region and below we provide the relevant quantities that are measured from EMD simulations,  
*Hydrodynamic slip:* (i) Fluctuations of the tangential component of the force acting on the slab due to the wall [compute

group/group]. (ii) The tangential component of the relative velocity between the wall and the slab (equivalently, the center-of-mass velocity of the fluid particles within the interfacial region) [variable *vcm*].

*Thermal slip:* (i) Fluctuations of the heat flux vector component normal to the wall. (ii) The temperature difference between the slab of water immediately adjacent to the wall.

Listing 1: LAMMPS syntax for creating dynamic groups. Text in *italics* must be specified by the user accordingly as per the LAMMPS documentation.

```

1  region      slab_region_id block INF INF INF INF INF
   ↵ slab_zmin slab_zmax units box
2  group       slab_group_id dynamic fluid_region_id
   ↵ region slab_region_id every update_freq
3  variable    variable_id equal vcm(slab_group_id, x)
4  compute     compute_id slab_group_id group/group
   ↵ wall_group_id
5  fix        fix_id all ave/time 1 1 1 c_compute_id[1]
   ↵ v_variable_id output_filename mode scalar

```

Listing 2: LAMMPS syntax for creating dynamic groups, heat flux, and temperature difference calculation. Text in *italics* must be specified by the user accordingly as per the LAMMPS documentation.

```

1  region      slab_region_id block INF INF INF INF INF
   ↵ slab_zmin slab_zmax units box
2  group       slab_group_id dynamic fluid_group_id
   ↵ region slab_region_id every update_freq
3  compute     compute_id1 slab_group_id property/atom
   ↵ vz
4  compute     compute_id2 slab_group_id force/tally
   ↵ wall_group_id
5  variable    variable_id1 atom c_compute_id1*c_
   ↵ compute_id2[3]
6  compute     compute_id3 slab_group_id reduce sum v_
   ↵ variable_id1
7  compute     compute_id4 wall_group_id temp
8  compute     compute_id5 slab_group_id temp
9  variable    variable_id2 equal c_compute_id4*c_
   ↵ compute_id5
10 fix        fix_id all ave/time 1 1 1 c_
   ↵ compute_id3 v_variable_id2 output_filename mode
   ↵ scalar

```

### 3.3. Post-processing

After obtaining adequate data from the EMD simulations, as described in the previous section, we advance to the post-processing stage. In this stage, the data obtained from the EMD simulations are used to calculate the interfacial friction coefficient and/or Kapitza resistance. The workflow to extract the corresponding parameters are:

1. Perform the time correlation for the simulation data sets.
  - (a) Navier friction coefficient: Perform auto-correlation of the center-of-mass slab velocity dataset and cross-correlation between the force component and slab velocity datasets (Algorithm 2). The function defined in Algorithm 2 takes as input the total time series data for the quantities whose correlations are

to be computed. The total time series is divided into *no\_of\_sets* independent blocks, and the final correlation data is the average over these independent blocks. The output of this function consists of the raw time correlation data and the normalized correlation data.

(b) Kapitza resistance: Perform autocorrelation between the temperature difference data set and cross-correlation between the heat flux-temperature difference data set. The correlation analysis follows the same procedure and data-blocking approach outlined for the Navier friction coefficient in Algorithm 2.

2. Transform the correlation functions into the Laplace domain (Algorithm 3). Lines 6 and 7 of Algorithm 3 correspond to performing a numerical Laplace transform of a function  $f(t)$ .

3. Compute the hydrodynamic friction/thermal resistance,

(a) Navier friction coefficient: The Laplace transforms of the correlation functions are passed to the function(s) defined in Algorithm 4, where the function returns the value of the zero-frequency friction kernel  $\zeta_0$ , which, when divided by the wall surface area, will provide the interfacial friction coefficient ( $\xi_0$ ).

(b) Kapitza resistance: The Laplace transform of the correlation functions are passed to the functions, defined in Algorithm 5, where the function returns the value of the Kapitza resistance,  $R_k$ .

---

#### Algorithm 2 Function algorithm to compute time correlation between two datasets

---

```

1: function CORRELATE(no_of_sets, data1, data2)
2:   Assign L  $\leftarrow$  LEN(data1)
3:   Assign no_of_cols  $\leftarrow$  L/no_of_sets
4:   Split data1 and data2 into no_of_sets segments
5:   Define an empty array corr_array[ROWS, COLS],
   ROWS = no_of_sets and COLS = no_of_cols
6:   for each j from 1 to no_of_sets do
7:     Assign a  $\leftarrow$  data1[j], b  $\leftarrow$  data2[j]
8:     Assign N  $\leftarrow$  LEN(a)
9:     Define an empty list corr = []
10:    for each k from 0 to N - 1 do
11:      Cab  $\leftarrow$   $\sum_{i=0}^{N-k-1} a[i] \cdot b[i+k] / (N - k)$ 
12:      Append Cab to corr
13:    end for
14:    Store corr in corr_array[ROW = j, :]
15:  end for
16:  Compute corravg  $\leftarrow$  ROW_MEAN(corr_array)
17:  Compute corravg_norm  $\leftarrow$  corravg / MAX(|corravg|)
18:  return corravg, corravg_norm
19: end function

```

---

---

**Algorithm 3** Function algorithm to compute numerical Laplace Transform

---

```

1: function LAPLACE(time, f_t, s_0, s_end, s_num)
2:   Assign  $\Delta t$ (timestep)  $\leftarrow \text{time}[1] - \text{time}[0]$ 
3:   Assign s values for the Laplace transform,
    $s \leftarrow \text{LINSPACE}(s_0, s_{\text{end}}, s_{\text{num}})$ 
4:   Define Lfs with array length = s_num
   for the Laplace transform data
5:   for each j from 0 to s_num do
6:     Assign  $e_{-st} \leftarrow \exp(-s[j] \cdot \text{time})$ 
7:      $Lfs[j] \leftarrow \int f_t \cdot e_{-st} \Delta t$ 
8:   end for
9:   return s, Lfs
10:  end function

```

---



---

**Algorithm 4** Function algorithm to compute the Navier friction coefficient

---

```

1: function METHOD1(Lcuu, Lcuf)
2:   Assign  $\zeta \leftarrow -Lcuf/Lcuu$ 
3:   return  $\zeta[0]$ 
4: end function

5: function METHOD2(frequ, Lcuu, Lcuf)
6:   Define the fitting model  $func \leftarrow -\frac{B}{s + \lambda}$  Lcuu
7:   Perform the regression fitting,
    $B, \lambda \leftarrow \text{CURVE\_FIT}(func, (frequ, Lcuu), Lcuf)$ 
8:   Assign  $\zeta_0 \leftarrow B/\lambda$ 
9:   return  $\zeta_0$ 
10:  end function

11: function METHOD3(s, Lcuu, Lcuf)
12:   Assign  $s_{\text{mid}} \leftarrow \text{LEN}(s)/2$  and  $s_{\text{last}} \leftarrow \text{LEN}(s)$ 
13:   Assign  $\Delta s \leftarrow s[1] - s[0]$ 
14:   Assign  $\Sigma_1 \leftarrow s[0]; \Sigma_2 \leftarrow s[s_{\text{mid}}]; \Sigma_3 \leftarrow s[s_{\text{mid}}];$ 
    $\Sigma_4 \leftarrow s[s_{\text{last}} - 1]$ 
15:   Assign  $A \leftarrow -Lcuu/Lcuf$ 
16:   Assign  $C \leftarrow \frac{\int_0^{s_{\text{mid}}} A[s] \Delta s}{\int_{s_{\text{mid}}}^{s_{\text{last}}} A[s] \Delta s}$ 
17:    $\lambda \leftarrow \frac{\Sigma_2^2 - \Sigma_1^2 + C(\Sigma_3^2 - \Sigma_4^2)}{2(C(\Sigma_4 - \Sigma_3) - \Sigma_2 + \Sigma_1)}$ 
18:    $B \leftarrow \frac{\Sigma_2^2 + 2\lambda_1\Sigma_2 - \Sigma_1^2 - 2\lambda_1\Sigma_1}{2 \int_0^{s_{\text{mid}}} A[s] \Delta s}$ 
19:    $\zeta_0 \leftarrow B/\lambda$ 
20:   return  $\zeta_0$ 
21: end function

```

---

**Algorithm 5** Function algorithm to compute the Kapitza resistance (proposed EMD framework)

---

```

1: function METHOD1(LcJqT, LcTT)
2:   Assign  $Gk \leftarrow LcTT/LcJqT$ 
3:   Assign  $Rk \leftarrow 1/Gk$ 
4:   return  $Rk[0]$ 
5: end function

6: function METHOD2(frequ, LcJqT, LcTT)
7:   Define the fitting model  $func \leftarrow \frac{B}{s + \lambda}$  LcTT
8:   Perform the regression fitting,
    $B, \lambda \leftarrow \text{CURVE\_FIT}(func, (frequ, LcTT), LcJqT)$ 
9:   Assign  $Gk0 \leftarrow B/\lambda$ 
10:  Assign  $Rk0 \leftarrow 1/Gk0$ 
11:  return  $Rk0$ 
12: end function

```

---

## 4. Results and Discussions

In this section, we present the results computed using the codes described in the previous section. We note that the figures have been reproduced using data from our previous studies on the Navier friction coefficient [16] and the Kapitza resistance [33]. For the hydrodynamic friction, we consider a planar water-graphene nanochannel, whereas for the thermal friction, we employ a water-CNT system.

### 4.1. Hydrodynamic slip

The first step in the post-processing stage is to compute the time-correlation functions defined in Eq. (1), and the function algorithm to calculate the time-correlation data using Python is provided in Algorithm 2. Fig 3 (a) shows an example of the time-correlation functions computed from the time series data of an EMD simulation of a water-graphene system. Further details about the simulation setup are provided in the Appendix A.1. Subsequently, the Laplace transforms of the time-correlation data can be computed using the algorithm shown in Algorithm 3, and inset plots of Fig 3 (a) show the Laplace transform of the corresponding time-correlation data.

Though while not specifically mentioned in Sec 2.1, the value for the Navier friction coefficient can be calculated using three different ways. For the first method, referred to as Method-1,  $\zeta_0$  is calculated directly as  $\tilde{C}_{u_x F_x}(0)/\tilde{C}_{u_x u_x}(0)$ , without assuming any functional form for the friction kernel, and the function METHOD1 in Algorithm 4 provides the algorithm to obtain the steady-state value of the friction kernel. For METHOD2 (function METHOD2 in Algorithm 4) a one-term Maxwellian function is assumed for the friction kernel (Eq. (4)), and the Maxwellian parameters are computed as the fitting coefficients of a regression fit of Eq. (5). Finally, Method-3 (METHOD3 in Algorithm 4) calculates the parameters in Eq. (3) from the algebraic expressions given via Eqs. (6)-(8). For Method-3, we chose the integral limits for the Laplacian domain in Eqs. (6) and (7) as  $s_1 = 0$ ,  $s_2 = s_3 = 0.5$ , and  $s_4 = 1$ .

As discussed in the Introduction, one of the commonly cited issues in calculating the Navier friction coefficient from

a Green-Kubo-like formalism [15] is the issue of the vanishing transport coefficient when integrated over long correlation times. To examine the effect of the correlation lag time in our approach, we compare the friction coefficient values calculated from the correlation functions truncated at different correlation lag times. Fig 3 (b) plots the friction coefficient values computed at different correlation lag times for a water-graphene system. Although all three methods show similar results for short lag times, the values for  $\xi_0$  calculated using Method-1 and Method-2 becomes statistically less reliable as the correlation lag time increases, whereas Method-3 shows consistent values of friction coefficient over the entire range of correlation lag times considered, with smaller statistical errors than Method-1 and Method-2. To quantify the statistical consistency of our methodology, we also plot a histogram distribution of the friction coefficient values over all the correlation lag times in Fig 3 (c) and observe that the least statistical dispersion is shown by Method-3. This suggests that error propagation in the computation of the friction coefficient is significantly smaller when using Method-3. We note that in our original work [16] we also compared the EMD results with the friction coefficient values computed from NEMD simulations. For the NEMD calculations, we simulated a Hagen–Poiseuille flow by applying an external field to the confined fluid and Fig 3 (d) shows the comparison of the friction coefficient values using different methodologies for a water-graphene system.

#### 4.2. Thermal Slip

The calculation of the Kapitza resistance in a cylindrical geometry is demonstrated using a CNT–water system. The slab of water adjacent to the CNT wall is defined as an annular region with a thickness of 3.165 Å, similar to the fluid slab thickness used in the graphene–water system. Figure 4 (a) compares the Kapitza resistance values obtained from both EMD and NEMD simulations. The EMD method offers a simpler and more flexible approach for cylindrical systems, as it is not limited by the CNT diameter. In contrast, the NEMD method requires additional modeling steps, such as introducing a smaller concentric CNT to generate a temperature gradient, which restricts the range of diameters that can be analyzed. Furthermore, two separate simulations are typically required in NEMD to account for the asymmetric heat flux in cylindrical geometries. Detailed modeling and simulation procedures for the NEMD calculations are available in our previous work [33]. The excellent agreement between the EMD and NEMD results confirms the validity and robustness of the present methodology for computing Kapitza resistance in cylindrical geometries.

Barrat and Chiaruttini developed an EMD approach based on the Green–Kubo formalism to evaluate Kapitza resistance for planar interfaces. In this work, we benchmark our EMD approach against their formulation and observe that our method does not suffer from the well-known plateau problem associated with Green–Kubo formalism of confined fluids [47]. Figure 4 (b) presents a comparison of the Kapitza resistance as a function of correlation time obtained using our EMD approach and the Green–Kubo-type method introduced by Barrat and Chiaruttini [48, 49]. While both approaches yield consistent values at short

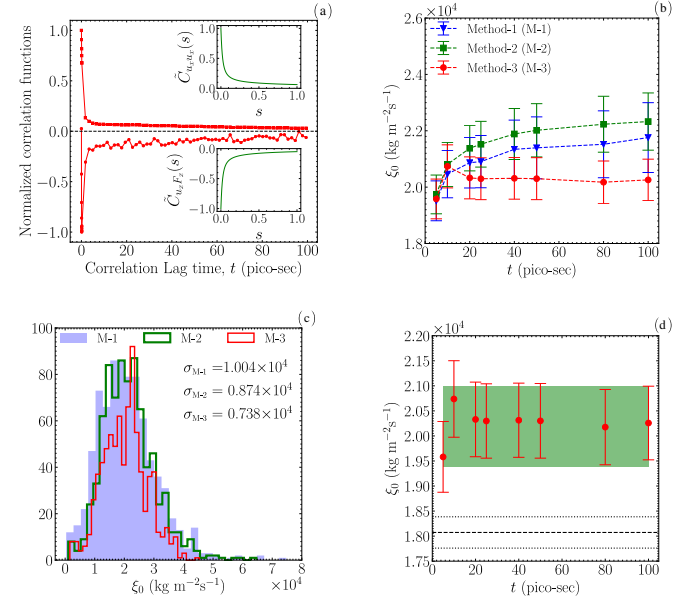


Figure 3: For a water-graphene system: (a) Normalized time correlation functions. Red filled squares represent  $C_{u_x u_x}(t)$ , and red filled circles represent  $C_{u_x F_x}(t)$ . The inset plot represents the corresponding normalized Laplace transform. (b) Variation of friction coefficient with correlation time intervals. The correlation lag times studied are  $t = 5, 10, 20, 25, 40, 50, 80$ , and 100 ps. The error bars correspond to one standard error obtained from 50 independent simulations. (c) Histogram distribution of friction coefficient values and  $\sigma$  represents the standard deviation of the distribution. (d) Comparison of  $\xi_0$  calculated using different methods. Red filled circles represent  $\xi_0$  calculated using Method-3 at different correlation lag intervals. The dashed line shows the  $\xi_0$  calculated using the methodology proposed in Ref 15 at the correlation lag time  $t = 5$  ps, and the dotted lines correspond to the upper and lower limits of the friction coefficient. The green shaded region represents the NEMD friction coefficient range at the external field  $\sim 1.25 \times 10^{11} \text{ ms}^{-2}$ . Reprinted with permission from Varghese *et al.* [16]. Copyright (2021) American Institute of Physics.

correlation times, the Green–Kubo-based method exhibits a divergence as the correlation time increases, whereas the results from our EMD method remain largely insensitive to the choice of correlation time. This robustness arises because our formulation directly correlates interfacial heat flux with temperature-difference fluctuations, thereby leveraging a larger fraction of the available simulation data. Furthermore, since the correlation functions are evaluated within an interfacial fluid region of thickness  $\Delta = 3.165 \text{ \AA}$  (measured from the CNT surface to the first peak in the water density profile), the resulting Kapitza resistance represents a local interfacial property rather than a bulk fluid property.

## 5. Conclusions

We have presented a computational framework from which the Navier friction coefficient (for velocity slip) and the Kapitza resistance (for thermal slip) can be evaluated using molecular dynamics simulations. The method is based on calculating the fluid equilibrium fluctuations in slabs adjacent to the walls, i.e., the local properties of the wall-fluid system are extracted. This, therefore, overcomes the size dependent problem

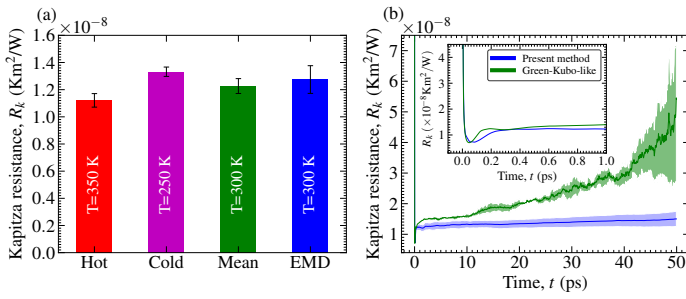


Figure 4: (a) Comparison of the Kapitza resistance obtained from the NEMD and the present EMD methods. (b) Comparison of the Kapitza resistance as a function of correlation time calculated using the present method and the Green-Kubo-like method of Barrat and Chiaruttini [48, 49]. Reprinted with permission from Alosios, *et al.* [33]. Copyright (2021) American Chemical Society.

present in other global system approaches. We have provided details showing how the relevant data can be extracted using LAMMPS. We also give the reader detailed algorithms for post-processing of the data to compute the Navier friction coefficient and Kapitza resistance. The method demonstrates superior accuracy and flexibility compared to existing EMD approaches, particularly in calculating Kapitza resistance in cylindrical geometries without the need for an auxiliary cylinder. Additionally, the present EMD method avoids the limitations of standard NEMD approaches for slip computation, which require extrapolation to zero strain rate or thermal gradient – a procedure that is particularly challenging for high-slip systems.

In any modeling effort of fluid or thermal flows at the nanoscale, precise knowledge about the boundary conditions can be critical [50]. We believe that the framework and the examples presented here can help researchers to obtain these quickly and efficiently.

## Appendix A. Simulation details

### Appendix A.1. Navier friction coefficient

The schematic illustration of the water-graphene system used for the EMD simulations is shown in Fig A.5. In Fig A.5 the graphene sheets are placed in the  $x - y$  plane with periodicity in both directions and confinement along the  $z$  axis. Each wall consists of three layers of stacked uncharged graphene sheets kept at an interlayer distance of 3.4 Å. The outermost layer at each wall is kept fixed to maintain a constant system size. The dimensions for the graphene nanochannel in the  $x - y$  plane are  $L_x = 36.87$  Å and  $L_y = 35.61$  Å. The intralayer carbon interactions for the graphene sheets were modeled using the optimized Tersoff potential [51, 52]. A weak Lennard-Jones potential is also applied between the interlayer carbon atoms to hold the graphene sheets together [38, 9].

To model the water molecules we use SPC/E [53, 54] water model with the bond and angles of each water molecule constrained using the SHAKE [55] algorithm in LAMMPS. Each hydrogen atom in the water molecule carries a partial charge of  $-0.4238e$ , and an oxygen atom carries a partial charge of  $-0.8476e$ , where  $e$  is the elementary charge of an electron.

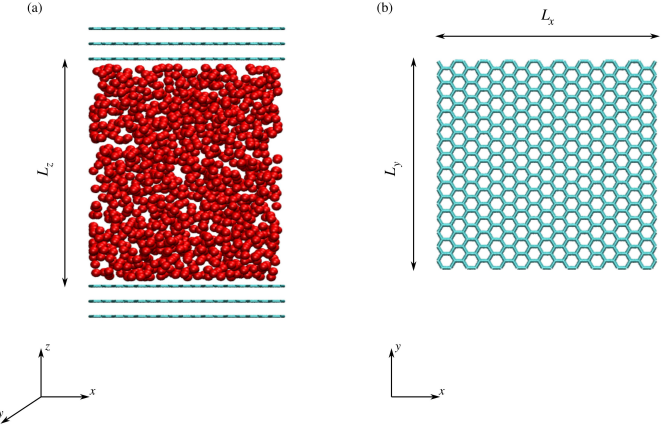


Figure A.5: (a) Schematic representation of the planar confined system. (b) Top view of the graphene channel. Reprinted with permission from Varghese *et al.* [16]. Copyright (2021) American Institute of Physics.

The van der Waals parameters for water-carbon (WC) interaction ( $\epsilon_{WC} = 0.09369$  kcal/mol,  $\sigma_{WC} = 3.19$  Å) are taken from Werder *et al* [56]. The Lennard-Jones parameters for oxygen-oxygen (OO) interaction are  $\epsilon_{OO} = 0.15535$  kcal/mol and  $\sigma_{OO} = 3.166$  Å, and Lennard-Jones interaction coefficients are zero for hydrogen atoms. The interaction cutoffs for Lennard-Jones and short-range Coulombic interactions were both kept at 10 Å. The long-range electrostatic interactions are calculated using the Ewald algorithm with the particle-particle-particle-mesh solver [57] of LAMMPS with a relative root mean square error in the per-atom force calculations below  $10^{-6}$ . To accommodate the non-periodicity in the  $z$  direction, we use the corrected Ewald algorithm EW3DC [58], where the ratio of extended volume to actual channel size is set as 3.0.

The equations of motion for all particles are integrated using the Velocity-Verlet [59] scheme of LAMMPS with an integration time step  $\Delta t = 1$  fs. To maintain an internal pressure of 1 bar the channel width is adjusted by fixing the bottom wall and using the top wall as a piston to apply pressure at 300 K. After setting the internal pressure, the water-graphene system is simulated for a total runtime of 6 ns. During the initial 2.0 ns, the system is equilibrated at 300 K by thermostating the walls using the Langevin thermostat [42]. The equilibration stage is followed by a 2.0 ns run in the NVE ensemble to verify the system stability, and the data required for the post-processing stage are collected from the final 2.0 ns run.

### Appendix A.2. Kapitza Resistance

The cylindrical system consists of water molecules confined inside a CNT and the schematic depiction of the initial configuration is shown in Fig. A.6. A (30,30) chiral CNT with a diameter of 4.06 nm is used in this particular case. The diameter of an (n,m) CNT can be calculated using the equation  $d = \sqrt{3}l/\pi \sqrt{n^2 + nm + m^2}$  where  $l=0.142$  nm is the carbon-carbon bond length. The initial configuration of the water-CNT system is created by immersing a rigid CNT in a water bath and equilibrating at 300K temperature and 1 bar pressure. This process will ensure the proper filling of water molecules inside the

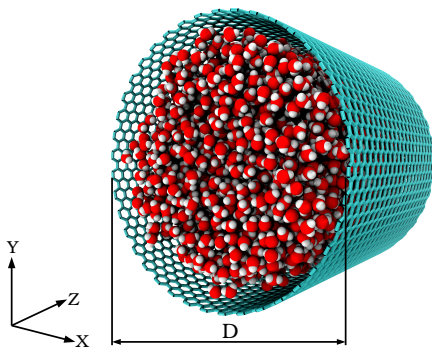
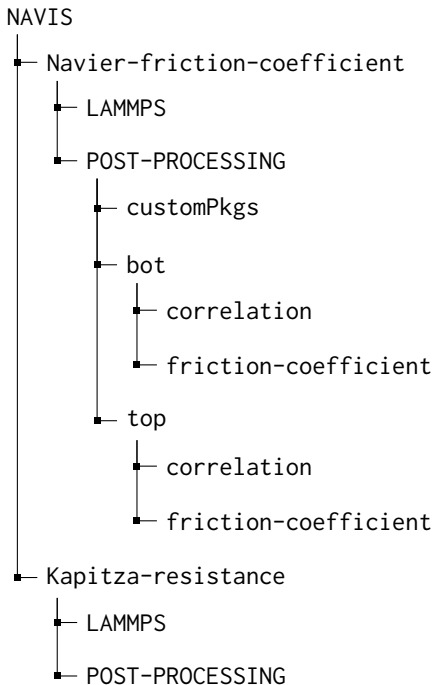


Figure A.6: Schematic diagram of water-CNT system. Reprinted with permission from Alosios, *et al.* [33]. Copyright (2021) American Chemical Society.

CNT. The final equilibrated system after removing the water molecules outside of CNT is used as the initial configuration for MD simulation. The water model used here is the same as that employed in the water-graphene system for the friction coefficient. The equations of motion for water and CNT were integrated using a leap-frog integration scheme with a time step  $\Delta t = 1$  fs. The simulation process involves minimization of the system followed by equilibration in canonical (NVT) ensemble for 2 ns at 300K temperature. Following that, the system stability was verified by a microcanonical (NVE) ensemble simulation for another 2 ns. For the production run, a thermostat is maintained at 300 K on the CNT for 5 ns, during which the necessary data is extracted.

## Appendix B. GitHub folder structure



## Acknowledgments

The results presented in this work was performed on the OzSTAR national facility at Swinburne University of Technology. The OzSTAR program receives funding in part from the Astronomy National Collaborative Research Infrastructure Strategy (NCRIS) allocation provided by the Australian Government, and from the Victorian Higher Education State Investment Fund (VHESIF) provided by the Victorian Government.

## Author declarations

### Conflict of interest

There is no conflict of interest to declare.

## References

- [1] K. Holmberg, A. Erdemir, The impact of tribology on energy use and co2 emission globally and in combustion engine and electric cars, *Tribol. Int.* 135 (2019) 389–396.
- [2] A. Sam, R. Hartkamp, S. Kumar Kannam, J. S. Babu, S. P. Sathian, P. J. Daivis, B. Todd, Fast transport of water in carbon nanotubes: a review of current accomplishments and challenges, *Mol. Simul.* 47 (10-11) (2021) 905–924.
- [3] L. Bocquet, E. Charlaix, Nanofluidics, from bulk to interfaces, *Chem. Soc. Rev.* 39 (3) (2010) 1073–1095.
- [4] A. Ajdari, L. Bocquet, Giant amplification of interfacially driven transport by hydrodynamic slip: Diffusio-osmosis and beyond, *Phys. Rev. Lett.* 96 (18) (2006) 186102.
- [5] A. Sam, R. Hartkamp, S. Kumar Kannam, J. S. Babu, S. P. Sathian, P. J. Daivis, B. Todd, Fast transport of water in carbon nanotubes: a review of current accomplishments and challenges, *Mol. Simul.* 47 (10-11) (2021) 905–924.
- [6] G. L. Pollack, Kapitza resistance, *Rev. Mod. Phys.* 41 (1) (1969) 48.
- [7] J. Chen, X. Xu, J. Zhou, B. Li, Interfacial thermal resistance: Past, present, and future, *Rev. Mod. Phys.* 94 (2) (2022) 025002.
- [8] B. D. Todd, P. J. Daivis, *Nonequilibrium Molecular Dynamics: Theory, Algorithms and Applications*, Cambridge University Press, 2017.
- [9] S. Kumar Kannam, B. D. Todd, J. S. Hansen, P. J. Daivis, Slip length of water on graphene: Limitations of non-equilibrium molecular dynamics simulations, *J. Chem. Phys.* 136 (2) (2012) 024705.
- [10] S. K. Kannam, B. D. Todd, J. S. Hansen, P. J. Daivis, How fast does water flow in carbon nanotubes?, *J. Chem. Phys.* 138 (9) (2013) 094701.
- [11] S. Bernardi, S. J. Brookes, D. J. Searles, D. J. Evans, Response theory for confined systems, *J. Chem. Phys.* 137 (7) (2012) 074114.

[12] S. Bernardi, D. J. Searles, Local response in nanopores, *Mol. Simul.* 42 (6-7) (2016) 463–473.

[13] L. Maffioli, E. R. Smith, J. P. Ewen, P. J. Daivis, D. Dini, B. D. Todd, Slip and stress from low shear rate nonequilibrium molecular dynamics: The transient-time correlation function technique, *J. Chem. Phys.* 156 (18) (2022) 184111.

[14] L. Maffioli, J. P. Ewen, E. R. Smith, S. Varghese, P. J. Daivis, D. Dini, B. Todd, Ttcf4lammps: A toolkit for simulation of the non-equilibrium behaviour of molecular fluids at experimentally accessible shear rates, *Comput. Phys. Commun.* (2024) 109205.

[15] L. Bocquet, J.-L. Barrat, Hydrodynamic boundary conditions, correlation functions, and kubo relations for confined fluids, *Phys. Rev. E* 49 (1994) 3079–3092.

[16] S. Varghese, J. S. Hansen, B. D. Todd, Improved methodology to compute the intrinsic friction coefficient at solid–liquid interfaces, *J. Chem. Phys.* 154 (18) (2021) 184707.

[17] P. Espanol, I. Zuniga, Force autocorrelation function in brownian motion theory, *J. Chem. Phys.* 98 (1) (1993) 574–580.

[18] D. J. Evans, G. P. Morriss, Statistical mechanics of nonequilibrium liquids, Academic Press, 1990.

[19] J. Petracic, P. Harrowell, On the equilibrium calculation of the friction coefficient for liquid slip against a wall, *J. Chem. Phys.* 127 (17) (2007) 174706.

[20] J. Brey, J. G. Ordóñez, Computer studies of brownian motion in a lennard-jones fluid: The stokes law, *J. Chem. Phys.* 76 (6) (1982) 3260–3263.

[21] L. Bocquet, J.-L. Barrat, On the green-kubo relationship for the liquid-solid friction coefficient, *J. Chem. Phys.* 139 (4) (2013).

[22] K. Huang, I. Szlufarska, Green-kubo relation for friction at liquid-solid interfaces, *Phys. Rev. E* 89 (2014) 032119.

[23] H. Oga, Y. Yamaguchi, T. Omori, S. Merabia, L. Joly, Green-kubo measurement of liquid-solid friction in finite-size systems, *J. Chem. Phys.* 151 (5) (2019) 054502.

[24] P. Español, J. A. de la Torre, D. Duque-Zumajo, Solution to the plateau problem in the green-kubo formula, *Phys. Rev. E* 99 (2019) 022126.

[25] H. Nakano, S.-i. Sasa, Statistical mechanical expressions of slip length, *J. Stat. Phys.* 176 (2019) 312–357.

[26] H. Nakano, S.-i. Sasa, Equilibrium measurement method of slip length based on fluctuating hydrodynamics, *Phys. Rev. E* 101 (2020) 033109.

[27] H. Oga, T. Omori, L. Joly, Y. Yamaguchi, Equilibrium molecular dynamics evaluation of the solid–liquid friction coefficient: Role of timescales, *J. Chem. Phys.* 159 (2) (2023) 024701.

[28] Theory of simple liquids, Academic Press, 2013.

[29] J. Petracic, P. Harrowell, Erratum: “On the equilibrium calculation of the friction coefficient for liquid slip against a wall” [J. Chem. Phys. 127, 174706 (2007)], *J. Chem. Phys.* 128 (20) (2008) 209901.

[30] J. S. Hansen, B. D. Todd, P. J. Daivis, Prediction of fluid velocity slip at solid surfaces, *Phys. Rev. E* 84 (2011) 016313.

[31] J.-L. Barrat, F. Chiaruttini, Kapitza resistance at the liquid–solid interface, *Mol. Phys.* 101 (11) (2003) 1605–1610.

[32] S. Alosious, S. K. Kannam, S. P. Sathian, B. D. Todd, Prediction of kapitza resistance at fluid-solid interfaces., *J. Chem. Phys.* 151 (19) (2019) 194502.

[33] S. Alosious, S. K. Kannam, S. P. Sathian, B. D. Todd, Nanoconfinement effects on the kapitza resistance at water-cnt interfaces., *Langmuir* 37 (7) (2021) 2355–2361.

[34] Python 3.12.2 documentation.

[35] A. P. Thompson, H. M. Aktulga, R. Berger, D. S. Bolintineanu, W. M. Brown, P. S. Crozier, P. J. in 't Veld, A. Kohlmeyer, S. G. Moore, T. D. Nguyen, R. Shan, M. J. Stevens, J. Tranchida, C. Trott, S. J. Plimpton, Lammps - a flexible simulation tool for particle-based materials modeling at the atomic, meso, and continuum scales, *Comput. Phys. Commun.* 271 (2022) 108171.

[36] S. Alosious, S. K. Kannam, S. P. Sathian, B. D. Todd, Kapitza resistance at water–graphene interfaces, *J. Chem. Phys.* 152 (22) (2020) 224703.

[37] S. Alosious, S. K. Kannam, S. P. Sathian, B. D. Todd, Effects of electrostatic interactions on kapitza resistance in hexagonal boron nitride–water interfaces, *Langmuir* 38 (29) (2022) 8783–8793.

[38] S. K. Kannam, B. D. Todd, J. S. Hansen, P. J. Daivis, Slip flow in graphene nanochannels, *J. Chem. Phys.* 135 (14) (2011) 144701.

[39] S. Varghese, B. D. Todd, J. S. Hansen, Existence of a maximum flow rate in electro-osmotic systems, *J. Chem. Phys.* 161 (19) (2024).

[40] S. K. Kannam, B. Todd, J. S. Hansen, P. J. Daivis, Interfacial slip friction at a fluid-solid cylindrical boundary, *J. Chem. Phys.* 136 (24) (2012).

[41] D. Frenkel, B. Smit, Understanding molecular simulation, Elsevier, 1957.

[42] M. P. Allen, D. J. Tildesley, Computer simulation of liquids, Oxford university press, 2017.

[43] A. P. Thompson, H. M. Aktulga, R. Berger, D. S. Bolintineanu, W. M. Brown, P. S. Crozier, P. J. In't Veld, A. Kohlmeyer, S. G. Moore, T. D. Nguyen, et al., Lammps-a flexible simulation tool for particle-based materials modeling at the atomic, meso, and continuum scales, *Comput. Phys. Commun.* 271 (2022) 108171.

[44] S. Bernardi, B. Todd, D. J. Searles, Thermostating highly confined fluids, *J. Chem. Phys.* 132 (24) (2010).

[45] S. De Luca, B. Todd, J. S. Hansen, P. J. Daivis, A new and effective method for thermostating confined fluids, *J. Chem. Phys.* 140 (5) (2014).

[46] A. Sam, S. K. Kannam, R. Hartkamp, S. P. Sathian, Water flow in carbon nanotubes: The effect of tube flexibility and thermostat, *J. Chem. Phys.* 146 (23) (2017).

[47] P. Espa  ol, J. de la Torre, D. Duque-Zumajo, Solution to the plateau problem in the green-kubo formula, *Phys. Rev. E* 99 (2) (2019) 022126.

[48] R. Puech, G. Bonfait, B. Castaing, Mobility of the 3he solid-liquid interface: Experiment and theory, *J. Low Temp. Phys.* 62 (1986) 315.

[49] J.-L. Barrat, F. Chiaruttini, Kapitza resistance at the liquid-solid interface, *Mol. Phys.* 101 (11) (2003) 1605–1610.

[50] J. S. Hansen, Nanoscale Hydrodynamics of Simple Systems, Cambridge University Press, Cambridge, 2022.

[51] J. Tersoff, Modeling solid-state chemistry: Interatomic potentials for multicomponent systems, *Phys. Rev. B* 39 (8) (1989) 5566.

[52] L. Lindsay, D. Broido, Optimized tersoff and brenner empirical potential parameters for lattice dynamics and phonon thermal transport in carbon nanotubes and graphene, *Phys. Rev. B* 81 (20) (2010) 205441.

[53] H. Berendsen, J. Grigera, T. Straatsma, The missing term in effective pair potentials, *J. Phys. Chem.* 91 (24) (1987) 6269–6271.

[54] Y. Wu, H. L. Tepper, G. A. Voth, Flexible simple point-charge water model with improved liquid-state properties, *J. Chem. Phys.* 124 (2) (2006) 024503.

[55] J.-P. Ryckaert, G. Ciccotti, H. J. Berendsen, Numerical integration of the cartesian equations of motion of a system with constraints: molecular dynamics of n-alkanes, *J. Comput. Phys.* 23 (3) (1977) 327–341.

[56] T. Werder, J. H. Walther, R. Jaffe, T. Halicioglu, P. Koumoutsakos, On the water- carbon interaction for use in molecular dynamics simulations of graphite and carbon nanotubes, *J. Phys. Chem. B* 107 (6) (2003) 1345–1352.

[57] R. W. Hockney, J. W. Eastwood, Computer simulation using particles, crc Press, 2021.

[58] I.-C. Yeh, M. L. Berkowitz, Ewald summation for systems with slab geometry, *J. Chem. Phys.* 111 (7) (1999) 3155–3162.

[59] W. C. Swope, H. C. Andersen, P. H. Berens, K. R. Wilson, A computer simulation method for the calculation of equilibrium constants for the formation of physical clusters of molecules: Application to small water clusters, *J. Chem. Phys.* 76 (1) (1982) 637–649.